CHEMICAL ENGINEERING TRANSACTIONS
VOL. 103, 2023
A publication of AIDIC
The Italian Association of Chemical Engineering
Online at www.cetjournal.it
Guest Editors: Petar S. Varbanov, Panos Seferlis, Yee Van Fan, Athanasios Papadopoulos

ISBN 979-12-81206-02-1; **ISSN** 2283-9216
DOI: 10.3303/CET23103104

Simulation of Heat Transfer Process in a Novel Phase Change Material Used for Solar Thermal Energy Storage

Nicolas Cabrera[a], Víctor Alexis Lizcano-González[a], Viatcheslav Kafarov[a,*], Khamid Mahamov[b]

[a]Department of Chemical Engineering, Carrera 27 Calle 9, Universidad Industrial de Santander, Bucaramanga, Colombia
[b]Department of Mechanical and Construction Engineering, Sutherland Building Newcastle-upon-Tyne NE1 8ST, Northumbria University, United Kingdom
kafarov@uis.edu.co

Harnessing solar thermal energy involves the design and construction of systems for the collection, storage, and distribution of heat. Heat storage can be done by sensible heat or latent heat, with the latter being preferred due to the higher densities achievable. The design of a storage system must consider the properties of the phase change material to be used, such as temperatures and enthalpies of fusion and crystallisation, as well as aspects of the heat exchanger, such as materials, configuration, and surface area, among others. This paper presents the simulation of the melting process of hydrogenated palm stearin for its use as a phase change material of renewable origin. A two-dimensional rectangular shell-coil geometry was used. The influence of the coil geometry on the heat transfer rate was evaluated using a constant flow of 3 L/min and a temperature of 75 C for the heat transfer fluid. According to simulations using COMSOL Multiphysics®, the heat transfer increases considerably for configurations where natural convection is favoured. These maximum transfer rate configurations are characterised by allowing the liquid phase of the PCM to flow to the top of the system. Additionally, despite the increases in heat transfer, the limiting factor is strongly defined in the PCM, which generates small differences between the inlet and outlet temperature of the heat transfer fluid. These results allow for heat exchanger designs based on shell-coil systems that, in addition to heat transfer improvements, let for the reduction of construction costs and the use of additives or support matrices.

1. Introduction

Considering that global energy consumption exceeds the supply, efforts have been made to implement alternative energy sources, especially renewable energies. One such energy is solar, which is classified into photovoltaic and thermal. Solar thermal energy storage systems have been the aim of the study because they allow for storing and even supply heat when there is no solar radiation (Mahkamov et al., 2018). Energy storage can be of two types, sensible and latent heat, the latter being of preference because it provides higher energy storage density. Latent heat storage systems (LHTES) implement the use of a phase change material (PCM) that can change from solid to liquid state and vice versa at a nearly constant temperature (Agyenim et al., 2010). PCM can be organic or inorganic, being the organic ones the most interesting because of their renewable and non-polluting nature. Examples of this are fatty acids. For the design of LHTES, the properties of the phase change material, such as the temperature and enthalpies of fusion and crystallisation, as well as aspects of the heat exchanger, such as materials, configuration, surface area, among others, must be considered (Hyman, 2011). However, analysing each aspect of the system to determine which parameters improve the system performance requires extra costs, so mathematical models are an optimal solution for design (Dutil et al., 2011). Although different configurations exist for the LHTES, the PCM is often confined in a rectangular vessel due to its simple geometric (Hu et al., 2015). Madruga et al. (2018) studied the effect of natural convection on the melting profiles of tetracosane contained in a cube and with a heat source in the inferior wall, identifying that because of natural convection, the melting process is divided into (i) conductive regime, (ii) steady growth regime, (iii) coarsening regime and (iv) turbulent regime. Wang et al. (2022) implemented a lauric acid PCM

Paper Received: 01 June 2023; Revised: 03 July 2023; Accepted: 21 July 2023
Please cite this article as: Cabrera N., Lizcano-González V.A., Kafarov V., Mahamov K., 2023, Simulation of Heat Transfer Process in a Novel Phase Change Material Used for Solar Thermal Energy Storage, Chemical Engineering Transactions, 103, 619-624 DOI:10.3303/CET23103104

inside a cubic geometry and using an MHPA (Micro-heat pipe array) as a heat source and evaluated the effect of pure conduction and natural convection heat transfer, demonstrating a dimensionless correlation between the liquid fraction of the PCM, the Rayleigh number and a dimensionless time, that the heat transfer by natural convection strongly depends on the height of the system, observing that at low heights the profile of the solid/liquid interface (mushy zone) is only influenced by conduction.
Based on the above, the objective of this work is to study for the first time the melting process simulation of the PCM of hydrogenated palm stearin contained in a rectangular geometry and the effect of using a rectangular, square shell-coil tube in a latent thermal heat storage system. Considering conduction and natural convection in the heat transfer model with an inlet flow of 3 L/min and temperature of 75 ºC of the heat transport fluid. Additionally, the simulation results obtained in this study are validated by laboratory experimental results.

2. Numerical analysis

2.1 Physical model

The physical model is presented in Figure 1. and consists of a rectangular geometry built-in Plexiglas with 300x50x310 mm dimensions with wall thicknesses of 10 mm. The entire system is thermally insulated with expanded polystyrene. The back cover had 9 K type temperature sensors inserted. The heat transport fluid (HTF) used was water at an inlet temperature of 75 ºC and at a rate of 3 L/min, running inside a single-turn square shell-coil copper tube with an internal diameter of 10 mm and wall thickness of 1 mm. The PCM used was hydrogenated palm stearin with thermophysical properties listed in Table 1.

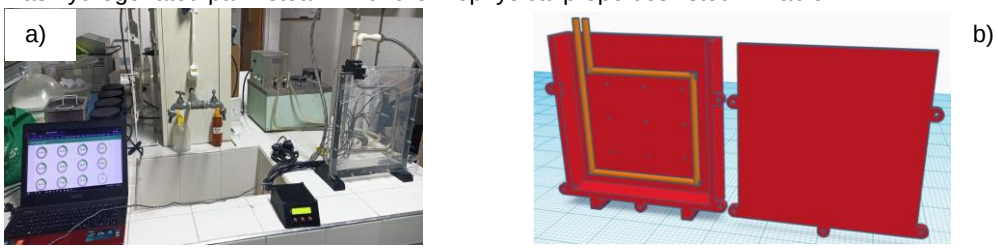

Figure 1: a) Experimental setup and b) 3D model designed in ThinkerCad

Table 1: Thermophysical properties of palm stearin

Property	Value	Property	Value
Melting point [T_M (ºC)]	53.5	Density (kg/m^3)	
Latent heat [L_h (kJ·kg^{-1})]	234	Solid [ρ_s]	1,026
Dynamic viscosity [μ (kg·m^{-1}·s^{-1})]	0.00689	Liquid [ρ_l]	820
Thermal conductivity (W·m^{-1}·ºC^{-1})		Heat capacity (J·kg^{-1}·ºC^{-1})	
Solid [k_s]	0.40	Solid [$C_{p,s}$]	1,850
Liquid [k_l]	0.40	Liquid [$C_{p,l}$]	2,384

2.2 Governing equations

The apparent heat capacity (AHC) method is employed to model the melting behaviour of PCM. The following assumptions are employed: PCM is isotropic but not homogeneous in its phases; liquid PCM is modelled as an incompressible Newtonian fluid; HTF and PCM are considered in laminar flow; heat loss in the boundary of the cover and temperature variation in the z direction of the PCM and fluid is negligible (2D geometry).
Equations used for the HTF are the Navier-Stokes equations and the energy equations, including heat transfer by convection and conduction, while for the PCM, the numerical analysis (Biwole et al., 2018) can be expressed with the continuity equation, Eq(1); x-momentum equation, Eq(2) and y-momentum equation Eq(3):

$$\frac{\partial \rho}{\partial x} + \frac{\partial \rho}{\partial y} = 0 \tag{1}$$

$$\rho \cdot \frac{\partial u}{\partial t} + \rho \cdot u \cdot \frac{\partial u}{\partial x} + \rho \cdot v \cdot \frac{\partial u}{\partial y} = -\frac{\partial p}{\partial x} + \mu \cdot \left[\frac{\partial^2 u}{\partial x^2} + \frac{\partial^2 u}{\partial y^2}\right] - A(T) \cdot u \tag{2}$$

$$\rho \frac{\partial v}{\partial t} + \rho \cdot u \cdot \frac{\partial v}{\partial x} + \rho \cdot v \cdot \frac{\partial v}{\partial y} = -\frac{\partial p}{\partial y} + \mu \cdot \left[\frac{\partial^2 v}{\partial x^2} + \frac{\partial^2 v}{\partial y^2}\right] - A(T) \cdot v + F_b \tag{3}$$

where ρ is the density, u is the velocity in the x-component, v is the velocity in the y-component, p is the pressure, μ is the dynamic viscosity, $A(T)$ is a term introduced to suppress the velocity in the solid phase of the PCM, expressed as the Carman-Kozeny equation for flow in a porous medium (Voller et al., 1987):

$$A(T) = C \cdot \frac{\left(1-\alpha(T)\right)^2}{\alpha(T)^3+\varepsilon} \tag{4}$$

where C is the Carman-Kozeny constant (also called the mushy zone constant) which depends on the medium studied and is arbitrarily high, in general between 10^3 to 10^{10}, taking for this study the value of 10^5, ε is a number used to avoid division by zero, commonly 0.001 (Biwole et al., 2013) and $\alpha(T)$ is the liquid fraction of the PCM, defined:

$$\alpha(T) = \begin{cases} 0 & T_m - \dfrac{\Delta T}{2} \le T \\ \dfrac{T-\left(T_m-\frac{\Delta T}{2}\right)}{\Delta T} & T_m - \dfrac{\Delta T}{2} < T < T_m + \dfrac{\Delta T}{2} \\ 1 & T \le T_m + \dfrac{\Delta T}{2} \end{cases} \tag{5}$$

The dynamic viscosity is expressed in terms of $A(T)$ to approximate the velocity to zero in the solid phase and in the region near the mushy zone, Eq(6); while the buoyancy force (F_b) is expressed in terms of the Boussinesq approximation Eq(7):

$$\mu = \mu_l \cdot \left(1 + A(T)\right) \tag{6}$$

$$F_b = \rho \cdot \beta \cdot g \cdot \left(T - T_{ref}\right) \tag{7}$$

where β is the coefficient of thermal expansion, ρ is the density in the liquid phase, g is the gravitational acceleration, T is the temperature and T_{ref} is the reference temperature ($T_{ref} = T_m$). The Energy equation was formulated as:

$$\rho \cdot c_\rho \cdot \left(\frac{\partial T}{\partial t} + u \cdot \frac{\partial T}{\partial x} + v \cdot \frac{\partial T}{\partial y}\right) = k\left(\frac{\partial^2 T}{\partial x^2} + \frac{\partial^2 T}{\partial y^2}\right) \tag{8}$$

where c_ρ is the heat capacity and k is the thermal conductivity. The thermophysical properties of PCM during phase change are defined:

$$\rho_{PCM} = (1-\alpha) \cdot \rho_s + \alpha \cdot \rho_l \tag{9}$$

$$k_{PCM} = (1-\alpha) \cdot k_s + \alpha \cdot k_l \tag{10}$$

$$C_{p,PCM} = (1-\alpha) \cdot C_{p,s} + \alpha \cdot C_{p,l} + L_h \cdot D(T) \tag{11}$$

where the subscripts *s* and *l*, are the solid and liquid phase. L_h is the latent heat of fusion and $D(T)$ is a Gaussian function in the interval between $T_m - \Delta T$ and $T_m + \Delta T$, used to distribute the latent heat equally around the melting point (Biwole et al., 2013), expressed:

$$D(T) = \frac{\mathrm{e}^{-\frac{(T-Tm)^2}{(\Delta T/4)^2}}}{\sqrt{\pi\left(\frac{\Delta T}{4}\right)^2}} \tag{12}$$

2.3 Initial and boundary conditions

Initial and boundary conditions applied are:

- Velocity equal zero ($v_{t=0} = 0$) and an ambient temperature ($T_{t=0} = 25\ ^0C$) in the system at an initial time.
- PCM is initially solid ($v_{t=0} = 0$) at room temperature ($T_{t=0} = 25\ ^0C$)
- Rate of 3 L/min and an inlet temperature of 75 ºC of the HTF.
- No-slip condition on the PCM walls and sides of the HTF ($v = 0$).
- Heat loss on the external walls of the system.
- Free surface on the upper wall of the PCM (Marangoni effect).

The mathematical model is solved in COMSOL Multiphysics® with the finite element method, employing a physics-controlled mesh with a finer size (Figure 2), with a total of 44,804 elements and consists of 39,286 triangular elements and 5,518 quadrilateral elements, with an average element quality of 0.8347. The simulation was solved on an Intel coreTM i7-8700 3.20GHz processor and 64 GB of RAM. The numerical solution strongly depends on the mesh size. Meshes larger than a normal size does not converge because the distances between nodes exceeds the width of the solid-liquid interface. Also, the results do not vary significantly with meshes smaller than finer size.

3. Results

3.1 Evolution of the melted PCM fraction

Figure 3 presents the melting fraction, where 0 is solid phase and 1 is liquid phase. The melting fraction is determined by a surface integration as follow:

$$MF = \frac{\iint Area\ with\ liquid\ phase\ dxdy}{Effectiveness\ area} \tag{13}$$

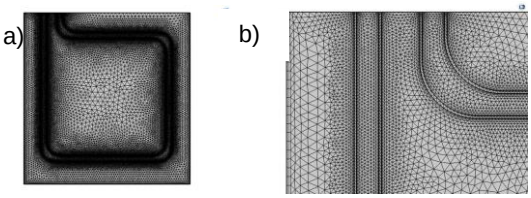

Figure 2: Demonstration of the mesh used. a) Complete 2D mesh and b) Ampliation zone

As shown in Figure 3, during the first 3 h approximately 70 % of the PCM melts, these being the zones most favoured by natural convection. Between 3 and 10 h a linear melting behaviour is observed, characterized by the fact that natural convection ceases to be predominant and heat transfer by conduction becomes more relevant. The melting process is completed at approximately 10 h, but according to the temperature profiles (Figure 4), the PCM melts in its entirety at about 11.5 h. This is because after 10 h of the experiment, the percentage of liquid PCM is less than 0.1 % and due to the low thermal conductivity of PCM and that the liquid fraction remaining is in the farthest zone from the heat source, this fraction takes about 1.5 h to melt.

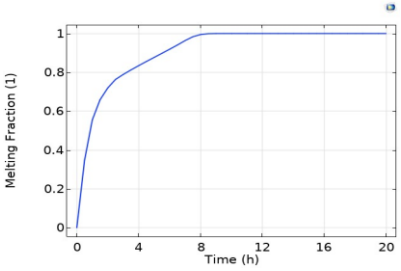

Figure 3: Melting fraction. It is observed that after 10 h of experimentation, complete melting of the PCM is achieved

Figure 4 presents the temperature profiles at different times (0.5, 1 and 10 h). The liquid fraction is the dark red colour and has a value of 1, the solid fraction is the blue zone and has a value of 0, and the mushy zone is the rainbow zone with values between 0 and 1. Heat transfer is dominated by conduction for up to 0.5 h. Natural convection starts to influence after 0.5 h. At 1 h the natural convection heat transfer is distinguished by favouring the melting of the PCM in the upper parts, while the lower zone is the last to melt. This melting is dominated by conductive heat transfer and because of the low thermal conductivity of the PCM, this zone melts in a significant time. After 10 h only the mushy zone exists, with values between 0.90 and 1.0.

3.2 Elements of validation

The validation is based on the comparison of the simulated and recorded temperature at the upper centre sensor of the experimental setup, Figure 5. It shows that the simulation has a good agreement with the experimental results. However, in the first 4 h of the test the temperatures present an error due to a significant increase in the ambient temperature, which reduced the heat losses of the experimental test. The PCM increases its

temperature exponentially, even when this temperature is above the phase change. The temperature remains constant at 65 ºC because of heat losses to the environment.
Another validation method was to compare the position of the simulated and real mushy zone or solid-liquid interface. Based on experimentation (Figure 5, b), the last zone to melt is the lower zone because of the low thermal conductivity of the solid phase of the PCM and because heat transfer did not favour the melting of this zone due to natural convection forcing the hotter liquid phase to rise continuously given their difference in densities. Although the simulation shows the effect of natural convection in these zones, the 2D modelling did not allow the natural convection to be calculated in conjunction with the centre of the system.

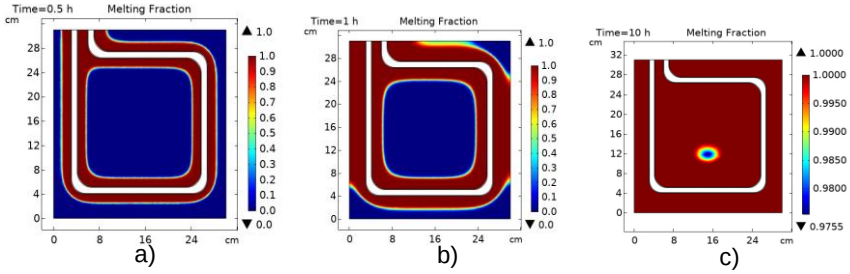

Figure 4: Melting fraction profiles at a) 0.5 h, b) 1 h and c) 10 h

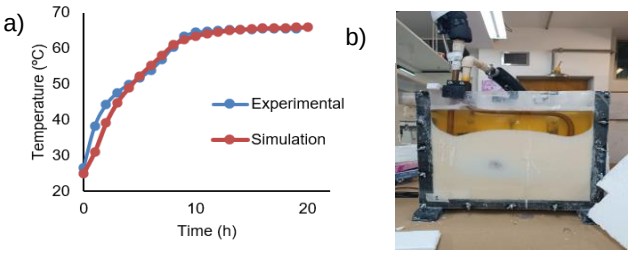

Figure 5: Elements of validation: a) Experimental and simulated temperatures and b) solid-liquid interface

3.3 Effect of the shell-coil geometry in the heat transfer

From the temperature profiles and melting times, the use of a single-turn square shell-coil melted the palm stearin more uniformly, favouring the effects of natural convection. However, it is necessary to establish an optimum distance between the walls and the centre, to improve the melting rate in the centre and the lower zone of the system, considering that those areas are the most critical. Compared to systems with a straight pipe (Bianco et al., 2022), the melting rate is faster, because there is a larger surface area of the HTF in contact with the solid PCM. Although, it is expected on a scale-up, coiled tubing allows for greater heat transfer between the HTF and the PCM, achieving optimal HTF outlet temperatures for domestic applications. The final shape achieved by the molten PCM and the correspondence of the simulation results with the experimental data show the strong influence of natural convection in vertical sections of the PCM, behaviour reported in the literature even for other exchanger configurations (Peng et al., 2020).

4. Conclusions

Hydrogenated palm stearin can be modelled with the mathematical model of apparent heat capacities, although it presents errors in initial times due to changes in the heat losses. Employing a single-turn square coil for the heat transport fluid in the solar thermal energy storage system melted the 70 % of the phase change material in approximately 3 h, favouring convective heat transfer. After this time, the melted rate is decreased because of the heat transfer is dominated by conduction and the PCM melted completely about 11 h. Due to heat losses, the maximum temperature reached by the PCM was around 65 ºC. The most critical zones are the central zone as it is the zone farthest from the heat source and the lower zone as it is dominated by conductive heat transfer. These zones being the most critical, their melting time will have a dependence on the heat loss to the environment. Therefore, due to heat losses, the time to melt the remaining 10% of the PCM in the central zone is about 2 hours. However, the use of a rectangular shell-coil geometry increases the surface contact area which causes the PCM to melt faster compared to other types of geometries. The temperature difference between the inlet and outlet of the HTF is 0.1 ºC. Although this difference is low, in a scale-up of the solar thermal energy storage system, the heat transfer between the HTF and the PCM will be more prolonged, so this temperature difference will be larger. These types of geometry require 3D modelling to discuss the combined effect of the

free convection of the lower zone with the central zone. Also, in a scaling up it would be recommended to study numerically the optimal distances between each turn of the pipe, favouring free convection.

Nomenclature

μ – dynamic viscosity, kg/(m·s)
C – Carman-Kozeny constant
C_p – specific heat capacity, J/(kg·ºC)
F_b – buoyancy force, N/m
k – thermal conductivity, W/(m·ºC)
L_h – latent heat, kJ/kg
p – pressure, atm
T – temperature, ºC
ΔT – melting range temperature, ºC
T_M – melting temperature, ºC
ρ – density, kg/m^3
u – velocity in the x-component, m/s
v – velocity in the y-component, m/s
x, y – cartesian coordinates
α - heat transfer coefficient, W/(m^2·ºC)
β – coefficient of thermal expansion, 1/ºC

subscripts
s – solid
l – liquid

Acknowledgments

Authors would like to thank The Royal Society for supporting this research through the Enabling Harvesting of Solar Energy for Remote Applications in the Andes Region (LA-SOLAR ENHANCE- ICA\R1\191201) project. Also special thanks to the Ministerio de Ciencia Tecnología e Innovación of Colombia for the support of the project entitled Desarrollo de una herramienta metodológica computacional y tecnologías de energías renovables para la transición energética en zonas de alta montaña en condiciones de post- pandemia, CD 82605 CT ICETEX 2022-0644.

References

Agyenim F., Hewitt N., Eames P.C., Smyth M., 2010, A review of materials, heat transfer and phase change problem formulation for latent heat thermal energy storage systems (LHTESS), Renewable & Sustainable Energy Reviews, 14(2), 615-628.

Bianco N., Graditi G., Fragnit A., Iasiello M., Mauro G.M., Mongibello L., 2022, Multi-objective optimization of a phase change material-based shell-and-tube heat exchanger for cold thermal energy storage: experiments and numerical modelling, Applied Thermal Engineering, 215, 119047.

Biwole P.H., Eclache P., Kuznik F., 2013, Phase-change materials to improve solar panel's performance. Energy and Buildings, 62, 59–67.

Biwole P.H., Groulx D., Souayfane F., Chiu T., 2018, Influence of fin size and distribution on solid-liquid phase change in a rectangular enclosure, International Journal of Thermal Sciences, 124, 433–446.

Dutil Y., Rousse D.R., Salah N.B., Lassue S., Zalewski L., 2010, A review on phase-change materials: Mathematical modeling and simulations, Renewable & Sustainable Energy Reviews, 15(1), 112-130.

Hu Z., Li A., Gao R., Yin H., 2015, A comparison study on melting inside the rectangular and curved unit with a vertical heating wall. Journal of Thermal Analysis and Calorimetry, 122(2), 831-842.

Hyman L.B., 2011, Sustainable thermal storage systems: planning, design, and operations. McGraw-Hill, New York, United States.

Madruga S., Haruki N., Horibe A., 2018, Experimental and numerical study of melting of the phase change material tetracosane. International Communications in Heat and Mass Transfer, 98, 163–170.

Mahkamov K., Pili P., Manca R., Leroux A., Mintsa A.C., Lynn K., Mullen D., Halimic E., Bartolini C.M., Pirro M., Costa S., Cabeza L.F., De Gracia Cuesto A., Kenisarin M., Makhkamova I., 2018, Development of a Small Solar Thermal Power Plant for Heat and Power Supply to Domestic and Small Business Buildings. Vol.1: Fuels, Combustion, and Material Handling; Combustion Turbines Combined Cycles; Boilers and Heat Recovery Steam Generators; Virtual Plant and Cyber-Physical Systems; Plant Development and Construction, Renewable Energy Systems, DOI:10.1115/POWER2018-7336.

Peng B., He Z., Wang H., Su F., 2020, Systematic investigations on charging performance enhancement of pcm-based thermal energy storage system by fin arrangements, Chemical Engineering Transactions, 81, 25–30.

Voller V.R., Prakash C., 1987, A fixed grid numerical modelling methodology for convection-diffusion mushy region phase-change problems, International Journal of Heat and Mass Transfer, 30(8), 1709–1719.

Wang Z., Diao Y., Zhao Y., Chen C., Wang T., Liang L., 2022, Visualization experiment and numerical study of latent heat storage unit using micro-heat pipe arrays: Melting process, Energy, 246, 123443.